ChemComm

Green Light Responsive Metal-Organic Frameworks for Colorectal Cancer Treatment

Journal:	*ChemComm*
Manuscript ID	CC-COM-01-2022-000591.R1
Article Type:	Communication

COMMUNICATION

Green Light Responsive Metal-Organic Frameworks for Colorectal Cancer Treatment

Received 00th January 20xx,
Accepted 00th January 20xx

DOI: 10.1039/x0xx00000x

Hannah D. Cornell,[a] Yumeng Zhu,[a] Stefan Ilic,[a] Naomei E. Lidman,[a] Xiaozhou Yang,[a] John B. Matson,[a] and Amanda J. Morris[a]*

Herein, the synthetic methods for preparation of a novel light-responsive metal-organic framework (MOF) UiO-AZB-F are outlined. Upon irradiation with green light, the framework demonstrates controlled release of chemotherapeutic drug cargo with simultaneous breakdown into low toxicity small molecule components.

In recent years, the field of nanomedicine has grown tremendously in an effort to improve patient outcomes.[1] Encapsulating therapeutics within nanocarriers can improve drug pharmacokinetics, enhance therapeutic efficacy, and reduce off-target effects through localized delivery of payload.[1a,2] Nanocarriers are particularly impactful in the field of oncology, as they present a strategy to selectively deliver cytotoxic anticancer drugs to the tumour region.[1a,3] A wide range of materials including peptides[4], polymers[5], and inorganic nanoparticles[6] have been developed towards this goal. Recently, metal-organic frameworks (MOFs)[7] have garnered interest as nanocarriers due to their chemical stability, high surface area, and tunable pore environments.[8] Through judicious choice of metal and linker, many low toxicity MOF systems have been successfully developed.[9]

For MOFs and other nanocarriers, controlling the release of therapeutic cargo can be challenging. To address this issue, many nanocarriers are designed with intrinsic stimuli-responsive elements. Internal stimuli, such as pH and redox environment, have been demonstrated as triggers for drug release.[5a] However, these parameters can vary from patient to patient, limiting their general effectiveness.[10] The use of external stimuli (light, ultrasound, magnetic field, etc.) may be more suited to a clinical setting, as it allows for spatiotemporal control and provides the ability to tailor treatment regimens to meet patient needs.[11]

Currently, there are several examples of FDA approved light-activated therapies, including photodynamic therapy (PDT) which is used for cancer treatment.[12] Through advances in light technologies, the scope of phototherapy targets[13] has widened in recent years. Lerch *et al*. developed a classification for organs (Classes 1-5) based on their photodruggability (i.e., general accessibility and ability to localize light delivery).[13c] Nearly all organs can be treated through relatively non-invasive methods such as endoscopy or minor incision.[13c] Red or near-IR responsive materials are commonly used for therapeutic applications to achieve maximum penetration into tissue. For superficial tumours, using shorter wavelength light sources can be beneficial.[14] Indeed, studies found using green light instead of red light as an irradiation source for PDT in the esophagus mitigated deep tissue damage while maintaining a high degree of clinical efficacy. Similar results are achieved in treating non-muscular invasive bladder cancers (NMIBCs). A ruthenium-based compound TLD-1433 has reached Phase II trials as a green light activated PDT photosensitizer.[15]

While many porphyrin-based MOF PDT photosensitizers[16] have been developed, methods for light-activated chemotherapy have been less explored in MOFs. In previous work[17], our lab developed the first light responsive MOF drug delivery vehicle (DDV) utilizing an azobenzene- based framework known as UiO-AZB. The zirconium framework contains photoswitchable 4,4'-azobenzenedicarboxylic acid (AZB) linkers. Upon irradiation with ultraviolet (UV) light, the MOF structure is destabilized, allowing for photo-controlled release of drug cargo. The design strategy allows for breakdown of the carrier upon light irradiation. Since unwanted nanoparticle accumulation is a concern, the ability to irreversibly degrade particles *in vivo* is advantageous for drug delivery applications.

While our previous work demonstrates promising "proof-of-concept," the use of UV light hinders clinical relevance. To this end, we developed a modified UiO-AZB framework that is responsive to green light. Herein, we report the synthesis of a new framework, UiO-AZB-F, which contains 4,4'-(diazene-1,2-

[a] *Department of Chemistry, Virginia Tech, Blacksburg, VA, USA*
*Corresponding Author Email: ajmorris@vt.edu
Electronic Supplementary Information (ESI) available: [details of any supplementary information available should be included here]. See DOI: 10.1039/x0xx00000x

diyl)bis(3,5-difluorobenzoic acid) (AZB-F) as the linker (Figure 1A). While some reports have utilized fluorinated azobenzene as pendant groups in MOFs[18], this work is the first of its kind to incorporate the compound into the backbone of a MOF.

The influence of substituents (specifically those occurring ortho to the azo bond) on the photophysical properties of azobenzene has been well documented in the literature.[19] To understand the role of *ortho*-tetrafluoro substitutions in our system, both AZB and AZB-F were synthesized *via* modified literature procedures (details available in ESI†).[17,20] The computational and experimental absorbance spectra of trans-dominant AZB and AZB-F compounds were investigated (Figure 1B). The compounds are characterized by two absorptions in the UV-Vis region of the spectrum. First, a strong π → π* transition can be observed at wavelengths < 400 nm. Second, the classic n→ π* absorption band occurs from 400–550 nm. The parent AZB exhibits a π → π* transition maximum at 331 nm. In AZB-F, this transition is slightly blue-shifted and occurs at 319 nm. The blue shift is also observed in our calculations and is due to destabilization of the HOMO (π* orbital)[19]. The molar absorptivity (Figure S5) at these wavelengths is similar for the parent and AZB-F derivatives (22,076 and 22,130 M^{-1} cm^{-1} respectively). For the n→ π* transitions, a weaker band is observed at 460 nm in the parent (ε ~545 M^{-1} cm^{-1}) and 465 nm (ε ~1372 M^{-1} cm^{-1}) in the fluorinated derivative. *Ortho*-fluorine substitutions reduce electron density near the N=N bond[19], resulting in a nearly 3-fold increase in absorptivity in the 400–550 nm range. Therefore, we can utilize the n→ π* band for green-light excitation. Indeed, after 15 min of constant irradiation (515 nm), *trans*-AZB-F is completely converted to its cis configuration, as evidenced by a change in the absorbance spectrum (Figure S6). Over the same irradiation time, no discernible trans-to-cis isomerization was observed for AZB with the same wavelength.

With the green-light responsiveness of AZB-F confirmed, the synthetic conditions for MOF preparation were optimized. Addition of modulators (monotopic ligands) is a common strategy employed to control MOF particle size during self-assembly. Therefore, a modulator screening (further synthetic details available in ESI†) was performed to determine optimal conditions for production of nanoscale MOF particles. In a general synthesis, 4,4'-(diazene-1,2-diyl)bis(3,5-difluorobenzoic acid) (0.1 mmol), $ZrCl_4$ (0.1 mmol), modulator (20–50 equiv.), and DMF were heated in a sealed vial at 120 °C (further details available in ESI†). The bulk structural purity of the resulting MOFs was confirmed using powder X-ray diffraction (PXRD) (Figure 2A and Figure S9). Interestingly, particles with higher crystallinity were obtained with shorter reaction time (15 min). SEM images revealed particles with octahedral geometry and appropriate size (< 200 nm) are obtained with formic acid modulation (Figure 2B). Consistently, dynamic light scattering (DLS) showed an average particle diameter of 150 ± 10 nm (Figure S12). The particles also exhibited a BET surface area of 1740 ± 30 m^2 g^{-1}. Despite the presence of fluorine within the pore space, the surface area is only slightly reduced (1900–2400 m^2 g^{-1} for UiO-AZB[17]) and pore volume is comparable, which indicates the particles have sufficient porosity for storage of drug cargo (Figure S13). Moreover, the modified pore environment and polar hydrophobicity imparted by fluorine atoms could enhance the affinity/uptake capacity of certain drug compounds.[21] Thermogravimetric analysis (TGA) shows that particles degrade above 450 °C (Figure S14), ensuring proper thermal stability of particles for our desired application.

After MOF characterization, the photo-switching behaviour of AZB-F bound within the crystalline lattice was investigated. MOF particles were placed in DMSO solution and irradiated with a 515 nm LED or heated at 37°C (normal physiological temperature) and kept in the dark. The absorbance of the supernatant was monitored *via* electronic absorption spectroscopy. In the irradiated sample, absorbance bands consistent with that of free AZB-F in solution appear over time (Figure 3A), indicating decomposition of UiO-AZB-F into its small molecule component (AZB-F^{2-}). When the MOF was heated under physiological conditions, negligible absorbance was observed over the course of 8 h, demonstrating the stability of particles under non-irradiative conditions at body temperature. The concentration of degraded MOF can be calculated over time (equation and further details available in ESI†). The percent degradation of the MOF was calculated by monitoring the absorbance at the isosbestic point to ensure total AZB concentration is measured. MOF degradation approaches 15% after 8 h, at which point the value plateaus due to reaching the solubility limit of AZB-F in solution. *In vivo* the degradation rate is unlikely to plateau, as the body experiences continuous flow due to the presence of biological fluids.

To demonstrate DDV capability, 5-fluorouracil (5FU) was selected as a model cargo. 5FU is a broad spectrum chemotherapeutic. Its small molecular size lends itself to successful incorporation within MOF pores.

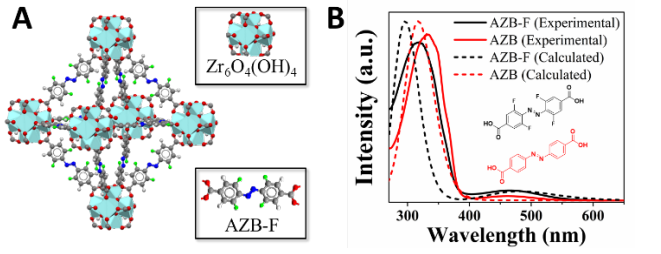

Figure 1. A) An octahedral cage of UiO-AZB-F (Zr: cyan, C: gray, O: red, F: green, H: white) **B)** Normalized experimental (solid) and simulated (dotted) absorbance data for AZB-F (black) and AZB (red) linkers

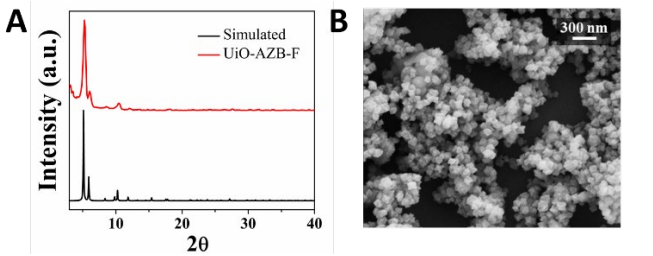

Figure 2. A) PXRD of UiO-AZB-F (formic acid, 20 eq.) compared to the simulated (black) crystal pattern (CCD #: 889532). **B)** SEM image of UiO-AZB-F particles (scale bar: 300 nm)

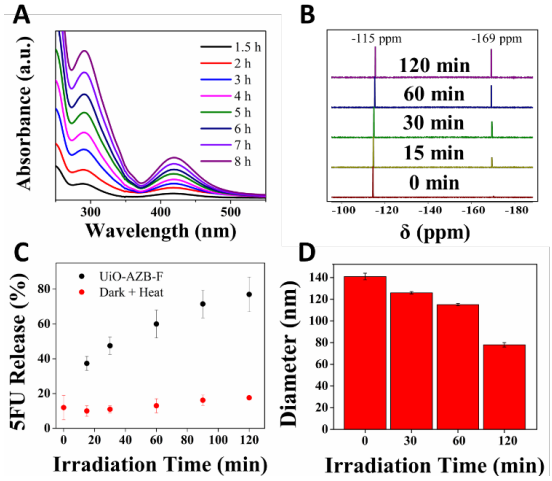

Figure 3. A) UV-Vis spectra used to probe degradation of UiO-AZB-F particles upon irradiation with green light. Over an 8 h period, the absorbance gradually increases, indicating release of free AZB-F into DMSO. **B)** Quantitative fluorine ^{19}F NMR spectra show a growing 5-fluorouracil peak (-169 ppm) with increased irradiation time. The internal standard peak (-115 ppm) was used to quantify the amount of 5FU released into aqueous solution. **C)** Plot of 5-fluorouracil release from UiO-AZB-F (as quantified by ^{19}F NMR) after green light irradiation (black) or heating in the dark (red). **D)** Dynamic light scattering (DLS) analysis of average particle size after various time points during the irradiation cycle. After 2 hours, the average particle diameter decreases by nearly 50%.

Three different loading procedures were explored to optimize 5FU incorporation. Drug loading was quantified using ^{19}F NMR spectroscopy, as both the MOF linker (AZB-F) and 5-fluorouracil contain fluorine. The first loading procedure was a post-synthetic impregnation method wherein MOF particles were suspended in a 3.5 mg/mL solution of 5FU and stirred for several days. The resulting loading values did not exceed 6 wt%. The second method employed ultrasonication during post-synthetic impregnation (further details in ESI†). The method achieved measurable loading with significantly decreased reaction times. A maximum loading of 10 wt% 5-FU was achieved after a 20 h sonication. The last method relied on an *in-situ* encapsulation method (details available in ESI†). 5FU was added to the reaction vial prior to MOF synthesis. PXRD of the resulting particles (Figure S17) showed that crystallinity was maintained during the modified procedure and further structural characterizations confirm retention of particle morphology (Table S2). Based on ^{19}F NMR spectroscopy, *in-situ* encapsulation gave comparable 5FU loadings (14 ± 4 wt%) to the ultrasonication method. A sharp decrease in available surface area was observed in drug loaded samples, which is consistent with drug molecules residing within the MOF pores rather than bound to the surface (Figure S18). With the substantial time savings (15 min vs. 20 h) the *in-situ* method provided, further studies used this method of loading. By eliminating the need for diffusion of cargo through a preformed structure, we propose that *in-situ* encapsulation may be a superior method to load other thermostable molecules.

Particles were further functionalized with amine-terminated PEG to increase aqueous stability and impart stealth properties. An amine moiety was selected due to its ability to coordinate to unsaturated Zr^{4+} sites within the framework. Addition of an amine functionality also allows for further modification of the particle surface to achieve selective uptake in cancer cells. Targeting moieties such as folic acid can be easily conjugated to the polymer through EDC/NHS coupling procedures (Figure S22). Particles were suspended in polymer solution for 24 h to achieve a maximum of 30 wt% coating (determined by ^{1}H NMR on an acid digested sample, Figure S23). The PXRD pattern (Figure S17) of PEGNH$_2$-UiO-AZB-F+5FU is broadened due to the significant contribution of amorphous polymer on the surface but maintains sharp diffraction peaks corresponding to MOF.

Controlled release of 5FU from PEGNH$_2$-UiO-AZB-F+5FU was investigated. Particles were suspended in aqueous solution and irradiated with 515 nm light for 2 h. After, the amount of 5FU released (Figure 3B) was quantified using ^{19}F NMR spectroscopy (with a known amount of 2,6-difluorobenzoic acid used as an internal standard). Only polymer functionalized particles were tested in these experiments, as surface modification mitigates large burst release upon immersion in solution.[17b] The release profile is show in Figure 3C. At time zero, particles show ~10% release of 5FU, which is attributed to burst from uncoated particles in solution. However, upon irradiation the rate of 5FU release increases dramatically, and 77 ± 10% of the encapsulated cargo was released in 120 min. The initial release rate from the PEGNH$_2$-UiO-AZB-F+5FU sample was calculated to be 0.91 ± 0.13% of total cargo per min. Comparatively, a control sample (kept in the dark with heating at 37 °C) shows minimal release of 5FU during the treatment window, demonstrating the stability of particles under non-irradiative conditions. Moreover, the data suggests that most cargo can be delivered within a few hours, making this method suitable for timely outpatient treatment.

To further probe the degradation mechanism, aliquots were taken for DLS analysis to measure the particle size at various timepoints throughout the treatment. The average particle diameter is presented in Figure 3D. Over the course of a two-hour treatment, the average particle size decreases by nearly half, supporting that particles photo-exfoliate upon isomerization of the incorporated ligand. The approach is clinically promising as the particles will break down in a timely manner rather than accumulate within organs.

With the success of our approach in solution, we sought to test the *in vitro* toxicity of our particles. A human colorectal cancer cell line (HCT-116) was selected. The colon is considered a Class 2 phototherapy target[13c], and easily accessible for light treatment. HCT-116 cells were seeded in a 96 well plate and treated with PEGNH$_2$-UiO-AZB-F (50, 100, and 200 μg/mL), or 20 wt% 5FU loaded PEGNH$_2$-UiO-AZB-F (50, 100, and 200 μg/mL). The cells were kept in the dark or subjected to cyclic irradiation treatment (further details available in ESI†) for 72 h. Cell viability was assessed using a CCK-8 assay, and the results are presented in Figure 4. Both PEGNH$_2$-UiO-AZB-F and PEGNH$_2$-UiO-AZB-F+5FU samples showed cell viability of ~80% in the dark, demonstrating minimal leakage of 5FU without irradiation. As MOF concentration increases, no differences in cell viability are observed, confirming the nontoxic nature of our material under control conditions (Figure S34). Under irradiative conditions, PEGNH2-UiO-AZB-F+5FU samples showed a sharp decrease in cell viability (<10%).

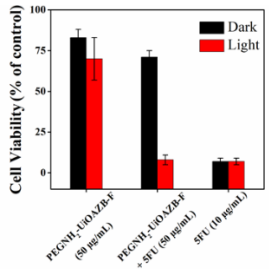

Figure 4. Cell viability data for HCT-116 cell line after treatment with $PEGNH_2$-UiO-AZB-F, $PEGNH_2$-UiO-AZB-F+5FU, or 5FU under dark (black) or irradiative (red) conditions.

In a 50 μg/mL sample loaded at 20 wt%, ~10 μg/mL of 5FU should be released into solution. The cell death observed from treatment with 50 μg/mL of drug loaded MOF and 10 μg/mL 5FU is within error, verifying that near quantitative payload is delivered. To evaluate if nanoparticles entered the cells or released 5FU extracellularly, we examined the cellular uptake of MOFs by ICP-MS (Figure S35). As the concentration of MOF increases, cellular uptake increases. Indeed, the cellular uptake of 200 μg/mL is around 2-fold higher than 50 μg/mL. These results verify that the MOFs enter cells.

In summary, we have detailed the preparation of a novel visible-light-activated MOF (UiO-AZB-F) that degrades into small molecule components upon green-light irradiation. The framework shows affinity for select chemotherapeutic cargo (5FU) and exhibits on-demand release. *In vitro* studies show light-induced drug release and cytotoxicity against a colorectal cancer cell line HCT-116. This study highlights the promise of MOF-based DDVs, specifically the precision and control that can be achieved using an external stimulus.

This work was supported by National Science Foundation Grant DMR-1551964. The authors acknowledge the Advanced Research Computing at Virginia Tech for providing computational resources and Virginia Tech's Materials Characterization Facility and Nanoscale Characterization and Fabrication Laboratory.

Conflicts of interest

There are no conflicts of interest.

Notes and references

1 *(a)* D. Kyung Kim and J. Dobson, *J. Mat.. Chem*., 2009, **19**, 6294–6307; *(b)* Y. H, Choi and H.K. Han, *J. Pharm. Investig*., 2018, **48**, 43–60; *(c)* S. Soares, S., J. Sousa, J., A. Pais, and C. Vitorino, C. *Front. Chem.* 2018, **6**.

2 F. Din, W. Aman, I. Ullah, O. S. Qureshi, O. Mustapha, S. Shafique, and A. Zeb, *Int. J. Nanomed.,* 2017, **12**, 7291–7309.

3 *(a)* V.P. Chauhan and R. K. Jain, *Nat. Mater.* 2013, **12**, 958–62; *(b)* R. Ranganathan, S. Madanmohan, A. Kesavan, G. Baskar, Y. R. Krishnamoorthy, R. Santosham, D. Ponraju, S. K. Rayala, and G. Venkatraman, *Int. J. Nano.* 2012, **7**, 1043–60.

4 A. Vedadghavami, C. Zhang, and A.G. Bajpayee, *Nano Today* 2020, **34**, 100898.

5 *(a)* Mura, S.; Nicolas, J.; Couvreur, P. Stimuli-Responsive Nanocarriers for Drug Delivery. *Nat. Mater.* **2013**, *12* (11), 991–1003; (b) S. R. MacEwan, D. J. Callahan, and A. Chilkoti, *Nanomed.,* **2010**, *5* (5), 793–806.

6 M. Liong, J. Lu, M. Kovochich, T. Xia, S. G. Ruehm, A. E. Nel, F. Tamanoi, and J. I. Zink, *ACS Nano,* 2008, **2**, 889–896.

7 H. Zhou, J.R. Long, and O. M. Yaghi, *Chem. Rev.* 2012, **112**, 673–674

8 *(a)* R. C. Huxford, J. D. Rocca, W. Lin, *Curr. Opin. Chem. Biol.* 2010, **14**, 262–268; *(b)* H. D. Lawson, S. P. Walton, and C. Chan, *ACS Appl. Mater. Int.,* 2021, **13**, 7004–7020.

9 *(a)* S. Muhammad, *Env. Sci. Poll. Res.,* 2016, **23**, 14805–7; *(b)* S. Wang, and C. Serre, *ACS Sus. Chem. & Eng.,* 2019, **7**, 11911–27.

10 *(a)* S. Wilhelm, A. J. Tavares, Q. Dai, S. Ohta, J. Audet, H. F. Dvorak, and W. C. W. Chan, *Nat. Rev. Mater.,* 2016, **1** , 1–12; (b) A. Raza, T. Rasheed, F. Nabeel, U. Hayat, M. Bilal, and H. M. N. Iqbal, *Molecules* 2019, **24** , 1117.

11 A. Raza, U. Hayat, T. Rasheed, M. Bilal, and H. M. N. Iqbal *J. Mater. Res. Technol.,* 2019, **8** , 1497–1509.

12 *(a)* S. Yano, S. Hirohara, M. Obata, Y. Hagiya, S. Ogura, A. Ikeda, H. Kataoka, M. Tanaka, and T. Joh. *J. Photochem. Photobio. C: Photochem. Rev.,* 2011, **12**, 46–67; *(b)* W. Fan, P. Huang, and X. Chen, *Chem. Soc. Rev.,* 2016, **45**, 6488–6519.

13 *(a)* W. A. Velema, W. Szymanski, and B. L. Feringa, *J. Am. Chem. Soc.,* 2014, **136**, 2178–91; *(b)* Z. Xie, T. Fan, J. An, W. Choi, Y. Duo, Y. Ge, B. Zhang, et al., *Chem. Soc. Rev.* 2020, **49**, 8065–87; *(c)* M. M. Lerch, M. J. Hansen, G. M. van Dam, W. Szymanski, and B. L. Feringa. *Angewandte Chemie Int. Ed.* 2016*,* **55**, 10978–99.

14 *(a)* P. Grosjean, G. Wagnieres, C. Fontolliet, H. van den Bergh, and P. Monnier, *Brit. J. Canc.* 1998, **77**, 1989–95; *(b)* V. H. S. vanRixel, B. Siewert, S. L. Hopkins, S. H. C. Askes, A. Busemann, M. A. Siegler, and S. Bonnet. *Chem. Sci.,* 2016, **8**, 4922–29; *(c)* S. Monro, K. L. Colón, H. Yin, John Roque, P. Konda, S. Gujar, R. P. Thummel, L. Lilge, C. G. Cameron, and S. A. McFarland. *Chem. Rev.,* 2019*.* **119**, 797–828.

15 More information on clinical trials available at ClinicalTrials.gov (identifier NCT03053635)

16 *(a)* G. Lan, K. Ni, and W. Lin, *Coord. Chem. Rev.*, 2019, **379**, 65–81; *(b)* W. Yu, W. Zhen, Q. Zhang, Y. Li, H. Luo, J. He, and Y. Liu, *ChemMedChem*, 2020, **15**, 1766–75; *(c)* J. Zhou, Y. Li, L. Wang, and Z. Xie,. *J. Mat. Chem. B.,* 2021, **9** , 7760–70.

17 *(a)* C. C. Epley, K. L. Roth, S. Lin, S. R. Ahrenholtz, T. Z. Grove, and A. J. Morris. *Dalton Trans.,* 2017, **46**, 4917–22; *(b)* K. Roth-Stefaniak, C. C. Epley, J. J. Novak, M. L. McAndrew, H. D. Cornell, J. Zhu, D. K. McDaniel, J. L. Davis, I. C. Allen, A. J. Morris, and T. Z. Grove. *Chem. Comm.,* 2018*,* **54**, 7617–20.

18 *(a)* S. Castellanos, A. Goulet-Hanssens, F. Zhao, A. Dikhtiarenko, A. Pustovarenko, S. Hecht, J. Gascon, F. Kapteijn, and D. Bléger, *Chem. Eur. J.*, 2016, 22, 746–52; *(b)* M. Rödl, S. Kerschbaumer, H. Kopacka, L. Blaser, F. R. S. Purtscher, H. Huppertz, T. S. Hofer, and H. A. Schwartz, *RSC Adv., 2021,* **11**, 3917–30; *(c)* A. B. Kanj, J. Bürck, N. Vankova, C. Li, D. Mutruc, A. Chandresh, S. Hecht, T. Heine, and L. Heinke, *J. Am. Chem. Soc.,* 2021*,* **43**, 7059–68.

19 *(a)* O. Sadovski, A. A. Beharry, F. Zhang, and G. A. Woolley. *Angewandte Chemie Int. Ed.,* 2009, **48**, 1484–86; *(b)* D. Bléger, J. Schwarz, A. M. Brouwer, and S. Hecht. *J. Am. Chem. Soc.,* 2012, **134**, 20597–600; *(c)* M. Dong, A. Babalhavaeji, S. Samanta, A. A. Beharry, and G. A. Woolley, *Acc. Chem. Res.,* 2015*,* **48**, 2662–70.

20 S. Okumura, C. Lin, Y. Takeda, and S. Minakata, *J. Org. Chem.,* 2013, **78**, 12090–105.

21 J. C. Biffinger, H. W. Kim, and S. G. DiMagno. *ChemBioChem*, 2004, **5**, 622–27.